Supplementary Information

High-strength Bone Polyurethane Adhesive with Rapid Curing for Bone Tissue Injury Repair

Xuehua Zhao[a,1], Jinju Ding[a,f,1], Chengkai Xuan[a,e], Jianing Liao[a], Xuetao Shi[a,b,c,d,*]

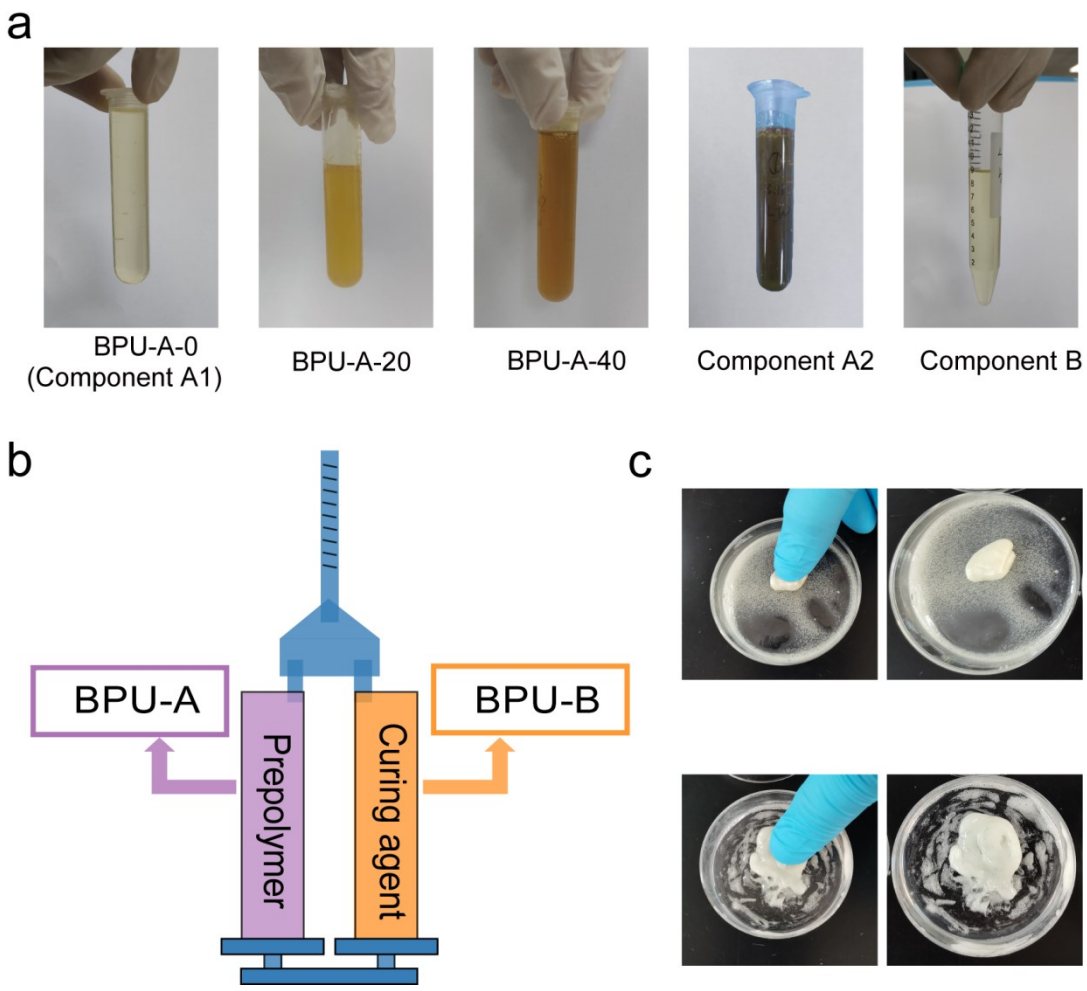

Fig. S1 (a) Synthesized polyurethane prepolymer; (b) two-component mixing syringe; (c) bone adhesive curing.

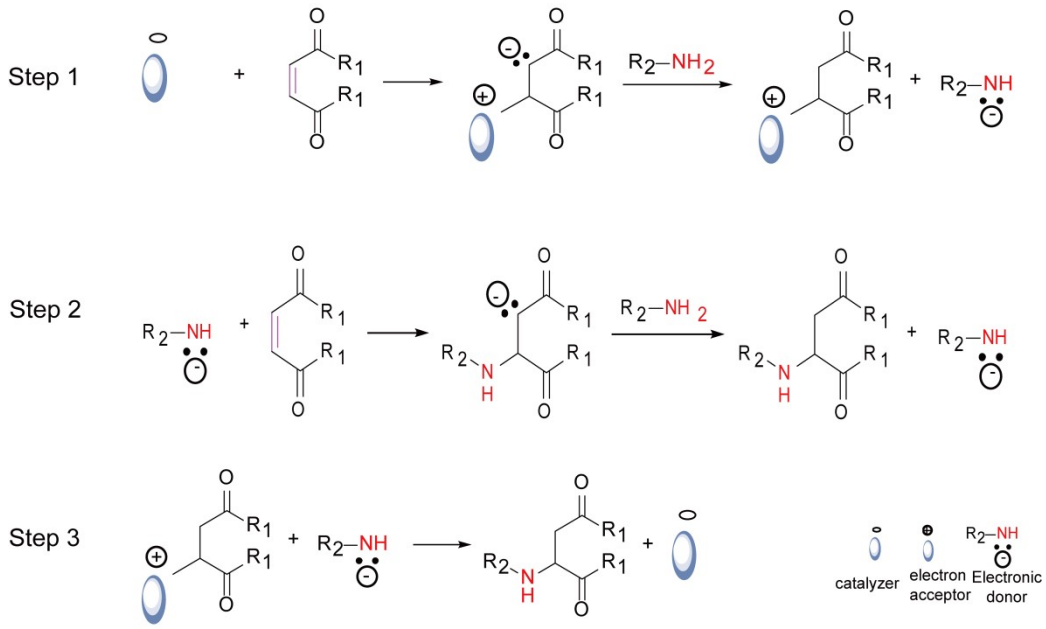

Fig. S2 Mechanism of the Michael addition reaction.

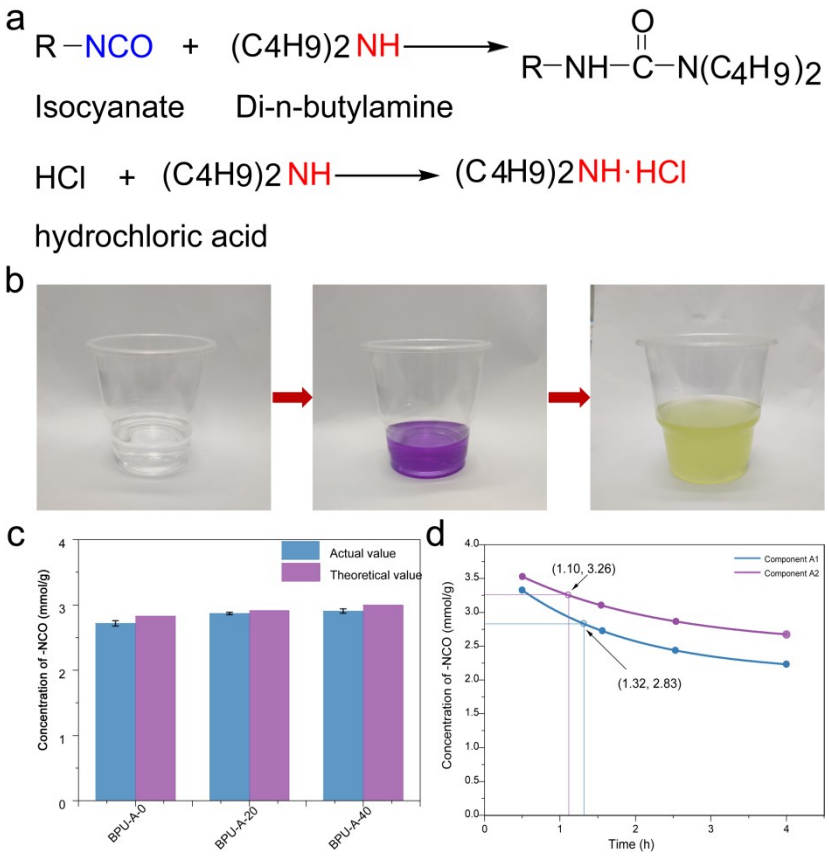

Fig. S3 Study of the NCO concentration. (a) Chemical equation for the dibutylamine- hydrochloric acid titration reaction; (b) color change during the titration process of the polyurethane prepolymer; (c) comparison of the actual and theoretical values of the -NCO concentration in BPU-As; (d) curve of the change in the -NCO concentration with reaction time.

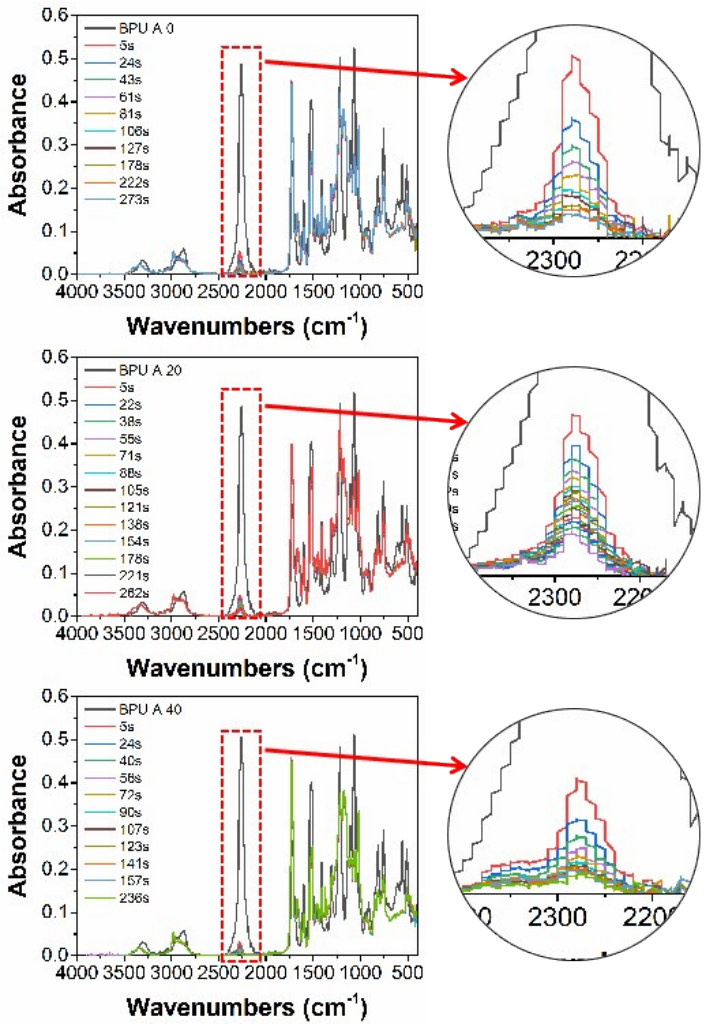

Fig. S4 Curing times of BPU-AB-0, BPU-AB-20, and BPU-AB-40.

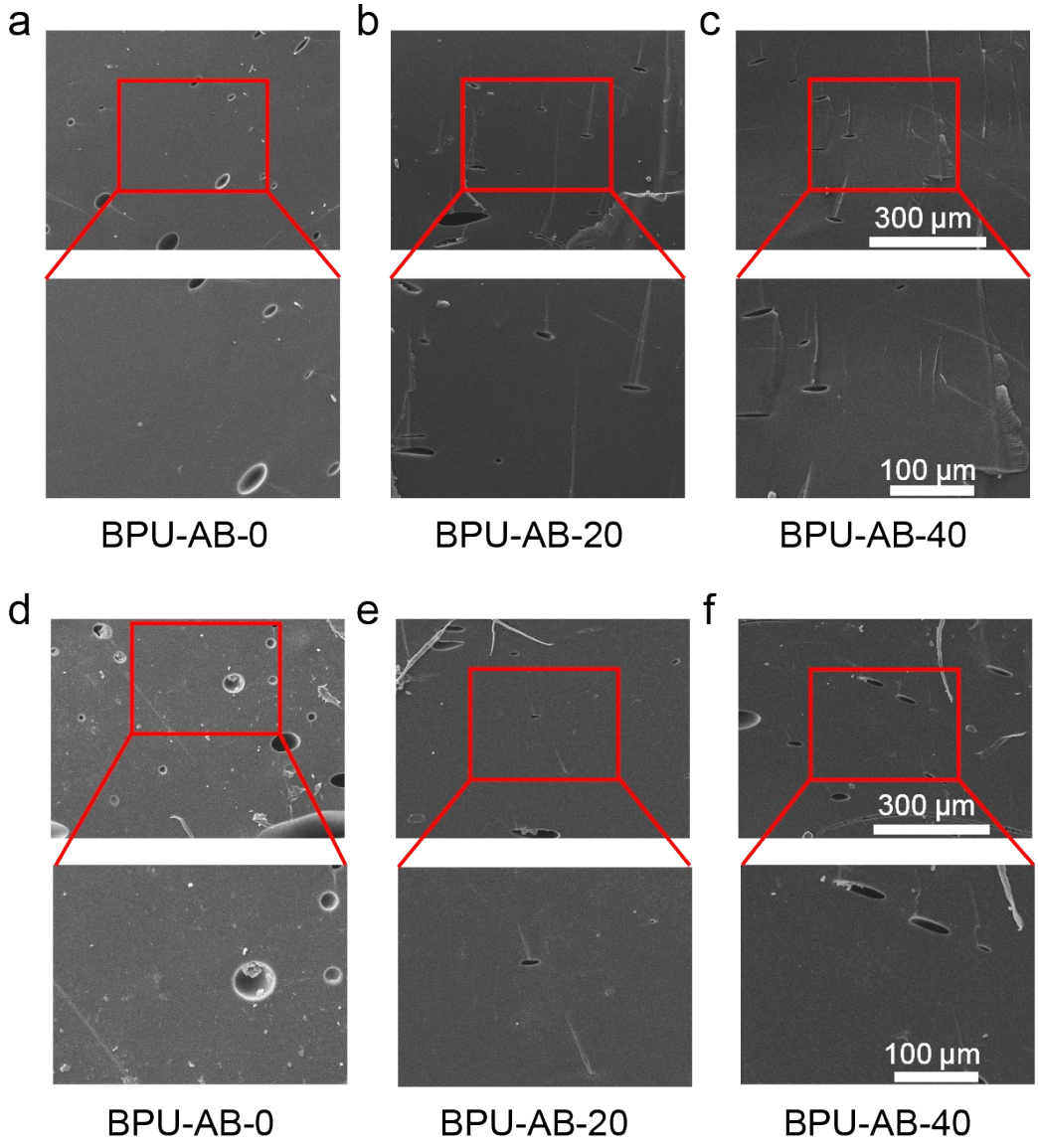

Fig. S5 Microstructure of BPU-ABs. (a) SEM images of the microstructure of the unswollen BPU-AB-0; (b) SEM images of the microstructure of the unswollen BPU-AB-20; (c) SEM images of the microstructure of the unswollen BPU-AB-40; (d) SEM images of the microstructure of BPU-AB-0 after water absorption and swelling; (e) SEM images of the microstructure of BPU-AB-20 after water absorption and swelling; (f) SEM images of the microstructure of BPU-AB-40 after water absorption and swelling.

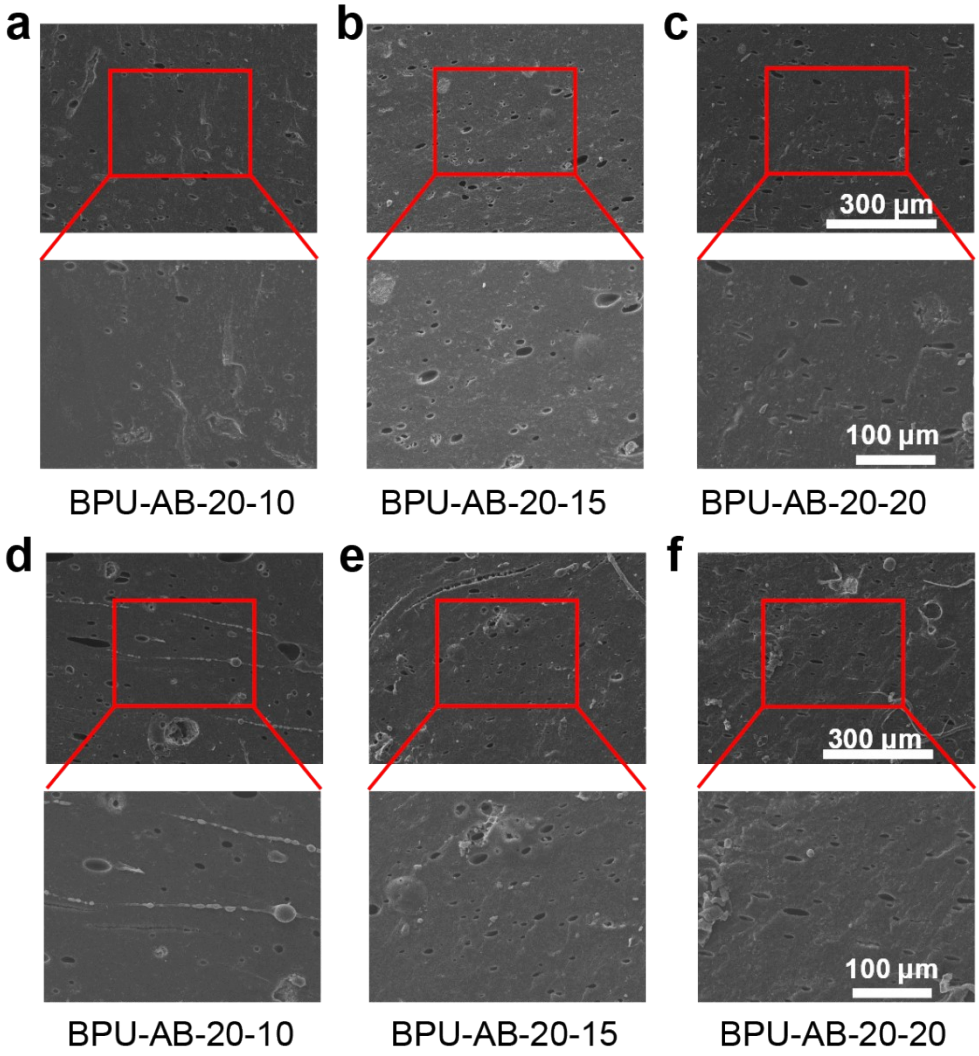

Fig. S6 Microstructure of BPU-AB-20s. (a) SEM images of the microstructure of the unswollen BPU-AB-20-10; (b) SEM images of the microstructure of the unswollen BPU-AB-20-15; (c) SEM images of the microstructure of the unswollen BPU-AB-20-20; (d) SEM images of the microstructure of BPU-AB-20-10 after water absorption and swelling; (e) SEM images of the microstructure of BPU-AB-20-15 after water absorption and swelling; (f) SEM images of the microstructure of BPU-AB-20-20 after water absorption and swelling.

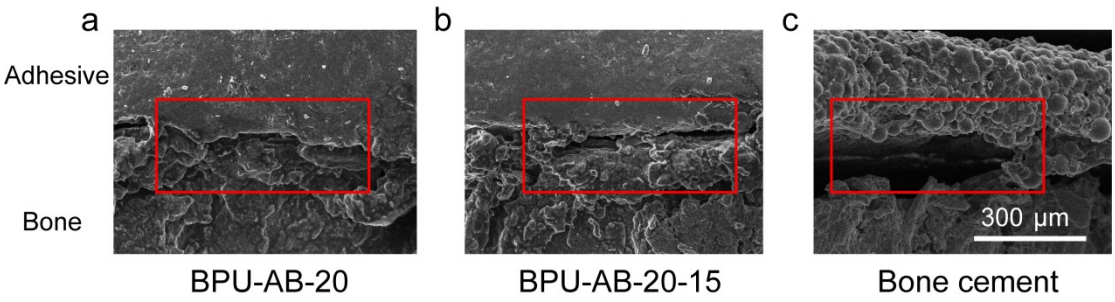

Fig. S7 Microstructure of the bonding interface. (a) SEM images of the bonding interface of BPU-AB-20 after the dynamic three-point tests; (b) SEM images of the bonding interface of BPU-AB-20-15 after the dynamic three-point tests; (c) SEM images of the bonding interface of the bone cement after the dynamic three-point tests.

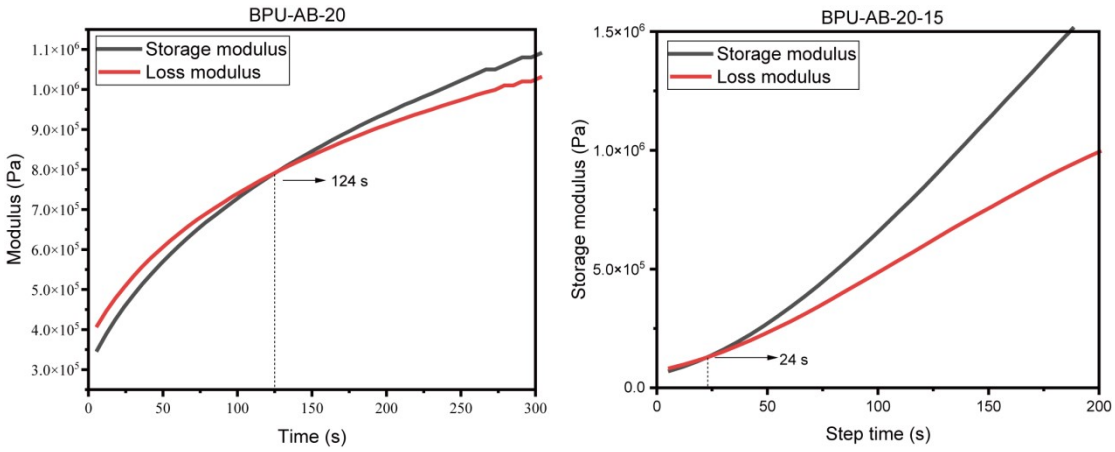

Fig. S8 Rheological testing of BPU-AB-20 and BPU-AB-20-15

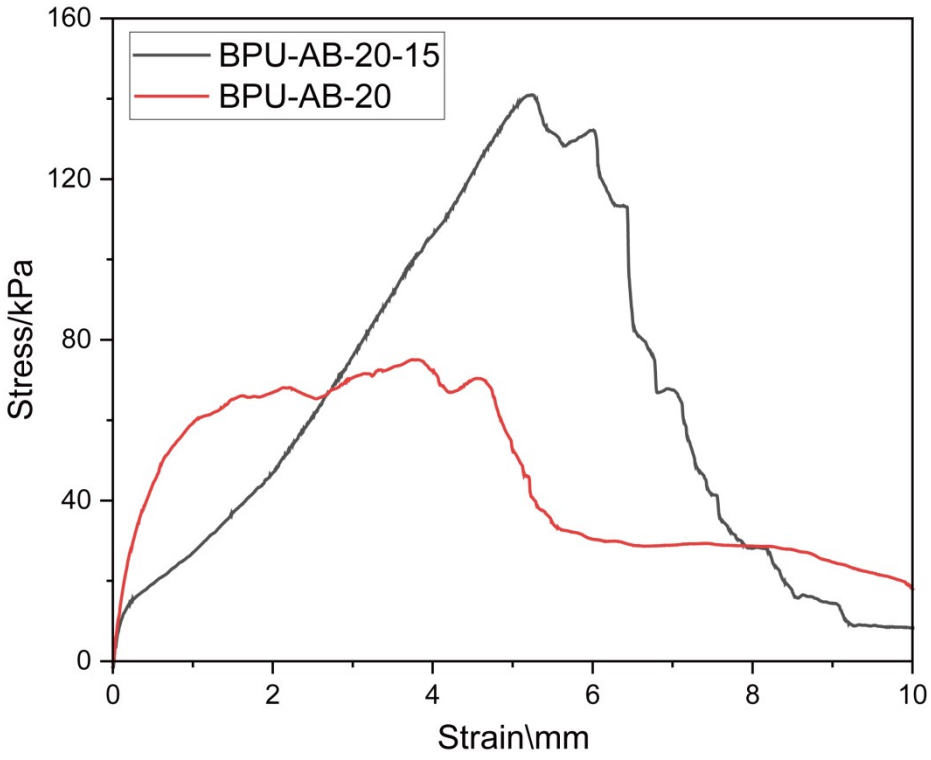

Fig. S9 Experiment on Overlapping Shear of Pig Skin with BPU-AB-20-15 and BPU-AB-20.

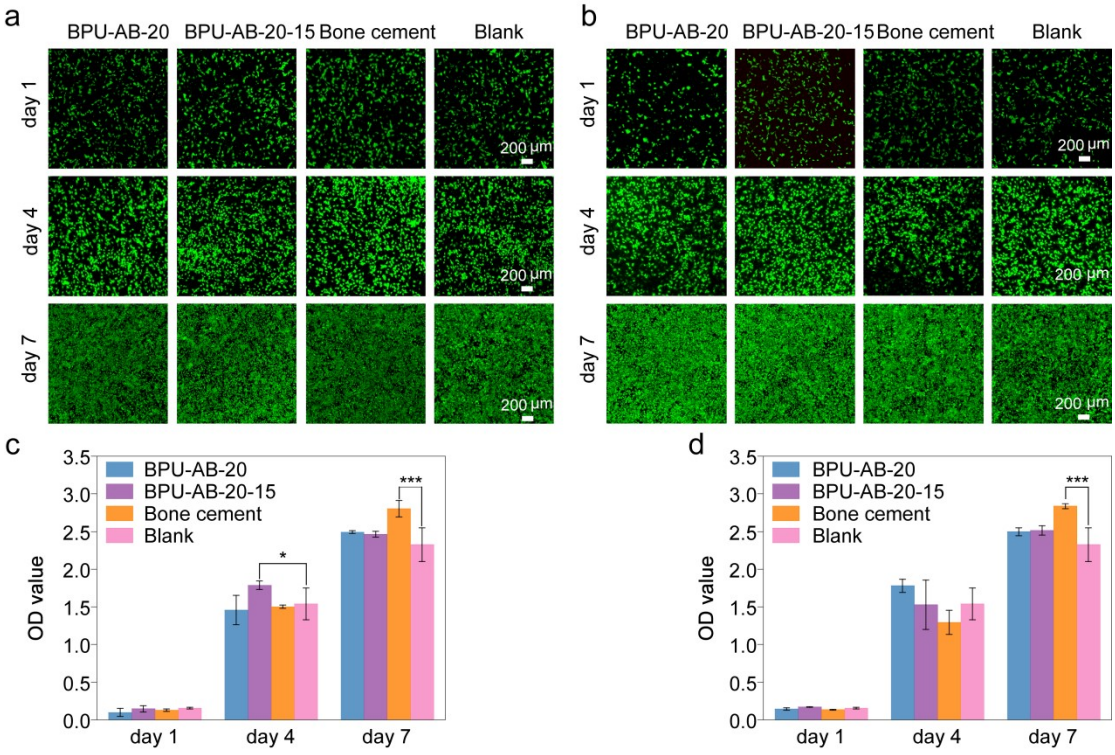

Fig. S10 In vitro biocompatibility evaluation. (a) Image of live/dead fluorescence staining of bone marrow stromal stem cells in a 10 mg/mL extraction mixture; (b) image of live/dead fluorescence staining of bone marrow stromal stem cells in a 20 mg/mL extraction mixture; (c) the results of the CCK-8 cell proliferation test in a 10 mg/mL extraction mixture; (d) cell proliferation in a 20 mg/mL extraction mixture; results of the CCK-8 cell proliferation assay. Significant difference (P value): * P <0.05, * * P <0.01, * * * P <0.001.

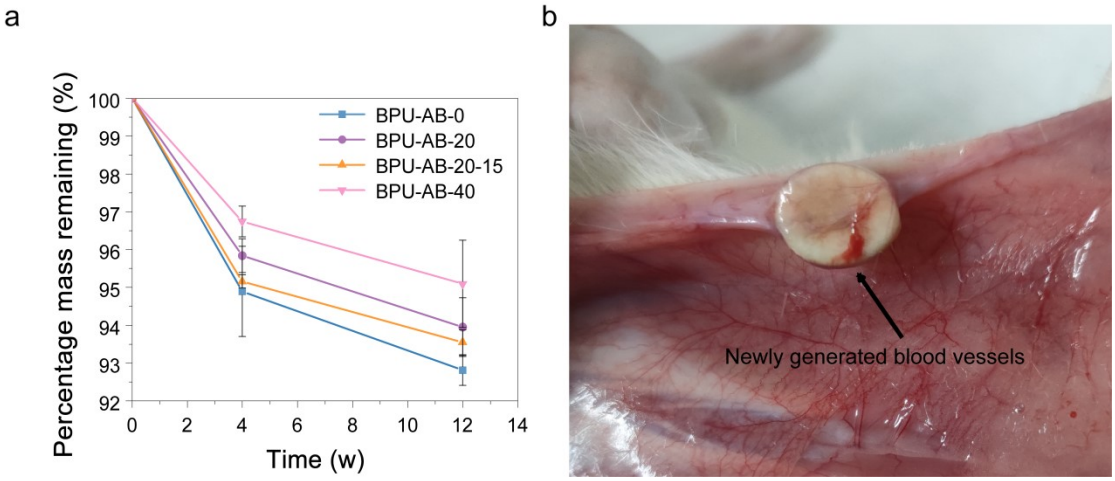

Fig. S11 In vivo degradation behavior of BPU-ABs implanted subcutaneously. (a) In vivo degradation curves of the BPU-ABs; (b) BPU-ABs implanted subcutaneously.

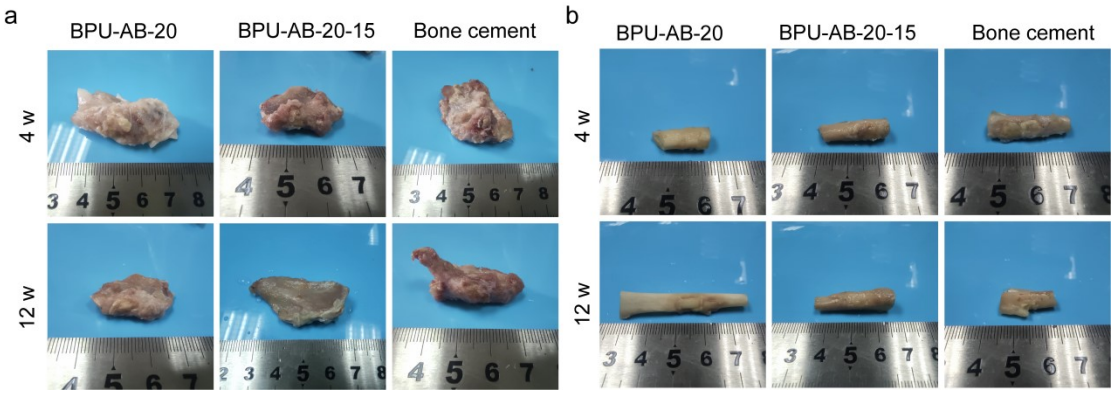

Fig. S12 (a) Recovery of iliac bone defects in New Zealand white rabbits at 4 and 12 weeks after surgery; (b) recovery of tibial defect sites in New Zealand white rabbits at 4 and 12 weeks after surgery.